Geomechanics and Engineering, *Vol. 22, No. 6 (2020) 553-564*
DOI: https://doi.org/10.12989/gae.2020.22.6.553

Solution for a circular tunnel in strain-softening rock with seepage forces

Luo Wei[1], Jin-feng Zou*[2] and Wei An[2]

[1]*Department of Civil Engineering, East China Jiaotong University, No.808, Shuanggang East Street, Nanchang, Jiangxi Province, People's Republic of China, 330013*
[2]*Department of Civil Engineering, Central South University, No.22, Shaoshan South Road, Central South University Railway Campus, Changsha, Hunan Province, People's Republic of China, 410075*

(Received February 7, 2020, Revised July 17, 2020, Accepted August 19, 2020)

Abstract. In this study, a simple numerical approach for a circular tunnel opening in strain-softening surrounding rock is proposed considering out-of-plane stress and seepage force based on Biot's effective stress principle. The plastic region of strain-softening surrounding rock was divided into a finite number of concentric rings, of which the thickness was determined by the internal equilibrium equation. The increments of stress and strain for each ring, starting from the elastic-plastic interface, were obtained by successively incorporating the effect of out-of-plane stress and Biot's effective stress principle. The initial value of the outmost ring was determined using equilibrium and compatibility equations. Based on the Mohr–Coulomb (M–C) and generalized Hoek–Brown (H–B) failure criteria, the stress-increment approach for solving stress, displacement, and plastic radius was improved by considering the effects of Biot's effective stress principle and the nonlinear degradation of strength and deformation parameters in plastic zone incorporating out-of-plane stress. The correctness of the proposed approach is validated by numerical simulation.

Keywords: strain-softening; out-of-plane stress; seepage force; new numerical procedure; surrounding rock; Biot's effective stress principle

1. Introduction

The stability analysis of surrounding rock in underground engineering is a fundamental and significant problem in engineering design (Jeffery 1921, Mindlin 1940, Atkinson and Pott 1977, Gonzalez and Sagaset 2001, Pinto and Whittle 2013, Golpasand *et al.* 2018, Rezaei *et al.* 2019, Aksoy *et al.* 2020, Zou *et al.* 2020, Zou *et al.* 2020, Qian *et al.* 2020, Zou and Zuo 2017, Chen *et al.* 2020, Chen and Zou, 2020, Xiao and Liu, 2017, Xiao *et al.* 2017, Xiao and Chen, 2020, Xiao *et al.* 2020, Li and Zhang 2020, Zhang *et al.* 2020, Zhang *et al.* 2020). Many methodologies have been proposed with different material constitutive models (e.g., elastic–perfectly plastic, elastic–brittle–plastic, and elastic strain-softening models) and strength criteria (e.g., Mohr–Coulomb (M–C) and generalized Hoek–Brown (H–B)). Although the published results have solved many of the engineering problems, the effect of out-of-plane stress has been neglected in most studies (e.g., Hoek and Brown, 2002, Carranza-Torres *et al.* 2004, Sharan 2008, Alonso *et al.* 2003, Nam and Bobet 2006, Lee and Pietruszczak, 2008, Ahamad and Mohammad, 2009). If the out-of-plane stress is neglected, the calculated stress will decrease, and the displacement will increase in the stability analysis of the surrounding rock. The calculation of the out-of-plane stress and determination of whether the out-of-plane stress is the major, intermediate or minor principle stress is an outstanding problem in strain-softening rock. Although the effect of the out-of-plane stress on the stress and displacement of surrounding rock has been discussed and some corresponding approach has been proposed for determining the out-of-plane stress, few published papers studies the effect of out-of-plane stress on the stress and displacement of strain-softening surrounding rock incorporating the seepage force based on Biot's effective stress principle. For example, Wang *et al.* (2012) considered the influence of out-of-plane stress on the distributions of stress, strain, and displacement based on the M–C failure criterion. But the seepage force is not taken into consideration is his study, which makes his solutions are not applicable for the water abundant area. Over decades, the solutions of steady seepage into a circular tunnel have also been investigated (Harr 1962, Schleiss 1986, Lei 1999, Bobet 2001, Aalianvari 2017, Farhadian *et al.* 2017).

In summary, the published literatures have principally focused on theoretical or numerical solutions for circular openings considering the single influencing factor among the strain-softening characteristic, out-of-plane stress and seepage force. Few studies on strain-softening surrounding rock have incorporated the effects of out-of-plane stress, seepage forces based on Biot's effective stress principle variation in the elastic strain of the plastic zone.

The main objective of this paper is to develop a simple numerical approach for a circular opening excavated in strain-softening rock masses. The numerical approaches are improved, and the computation procedures are performed incorporating Biot's effective stress and the out-of-plane stress, based on M–C and generalized H–B criteria. The

*Corresponding author, Professor
E-mail: zoujinfeng_csu@163.com

ISSN: 2005-307X (Print), 2092-6219 (Online)

number of annuli in the plastic zone and Biot's coefficient are selected to conduct an analysis of the parameters. The results of the proposed approach show satisfactory agreement with that of previous reports and numerical simulation.

2. Methodology

2.1 Statement of the problem

A circular opening of radius r_0 is excavated in a continuous, homogeneous, isotropic, and initially elastic rock mass subjected to hydrostatic pressure (σ_0) and an axial in situ stress (q) along the tunnel axis (Fig. 1).

In Fig. 1, an internal support pressure (p_{in}) uniformly acts on the tunnel wall surface in the radial direction after excavation. The stress and displacement of the surrounding rock depends on the radius of the cylindrical polar coordinate system without considering the gravity field. F_r is the seepage force along the radial direction of the tunnel. R is the plastic radius; R_s is the plastic radius for the softening region. $\overline{R}$ is the radius of the interface between the inner and outer plastic regions.

In this paper, Biot's effective stress principle is adopted for the rock mass (Bui *et al.* 2014, Detournay 1993). When considering the seepage flow surrounding tunnel, the deformation of rock is determined by Biot's effective stress (Biot and Wills 1957), defined as,

$$\sigma' = \sigma - \alpha_0 \mathrm{p_w} \tag{1}$$

where, σ' is Biot's effective stresses and σ is total stresses (radial and circumferential stresses) in surrounding rock, α_0 is the Biot's coefficient, and p_w is pore-water pressure. When α_0=1, the Biot's effective stress principle can be transformed to the famous Terzaghi's effective stress principle. The value of α_0 may reach 0.5 in a saturated pervious rock.

Much research has been conducted to determine the value of Biot's coefficient α_0 (Cosenza *et al.* 2002). Biot's effective stress principle is more widely applied to studies of rock mass than Terzaghi's effective stress principle based on historic research.

2.2 Assumptions

The following assumptions are made for studying the influence of the seepage force and out-of-plane stress on the stress and displacement around the circular opening excavated in the strain-softening rock mass. The rock mass around the circular opening is a homogeneous, isotropic, continuous, and permeable medium, and the seepage force is treated as body force. The hydrostatic pressure in the seepage field is assumed to be uniformly distributed in the radial direction. The rock masses surrounding the circular opening obey the M–C or the generalized H–B failure criterion under the plane-strain condition. The elastic–brittle–plastic and strain-softening constitutive models with a non-associated flow rule are employed for analysis. The elastic strain in the plastic region of the surrounding rock

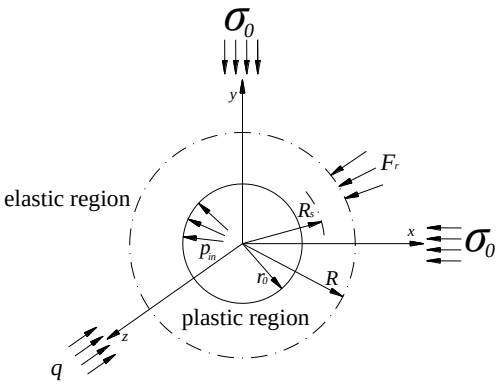

Fig. 1 Analytical model of the circular opening in a strain-softening rock mass

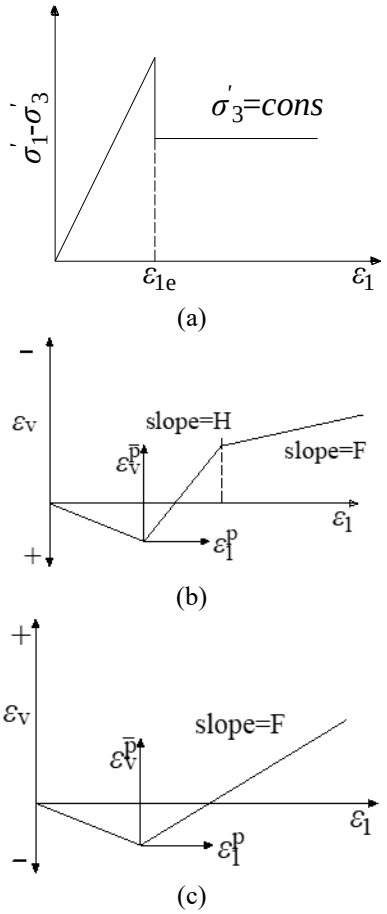

Fig. 2 Elastic-brittle-plastic material behaviour model

obeys Hooke's law. The strength parameters of the rock mass deteriorate with plastic deformation development after the post-peak-strength surface. The axial in situ stress is the axial stress and is defined as the out-of-plane stress in the paper (i.e., $q=\sigma_z'$). Compressive stress and direct strains are taken as positive. Biot's effective stress principle was adopted to conduct the analysis of tunnels below the groundwater table.

2.3 Elastic-brittle-plastic behaviour of the rock mass

The stress-strain relationship of the elastic-brittle-plastic

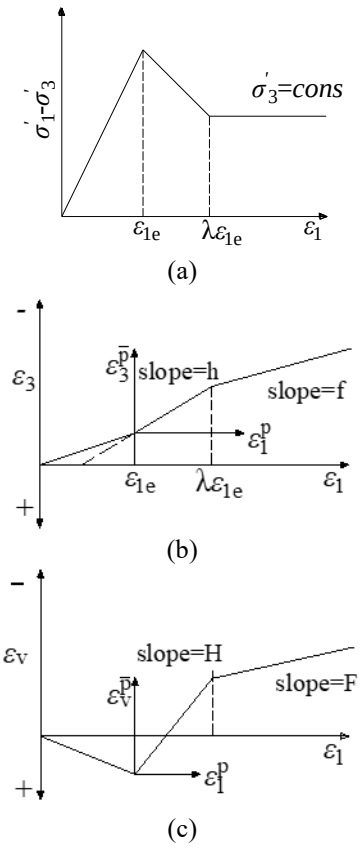

Fig. 3 Strain-softening material behaviour model

rock mass is presented in Fig. 2.

In Fig. 2, the rock mass strength decreases from peak to residual strength after yielding. σ'_1 and σ'_3 are the major and minor principal stresses, respectively. ε_r, ε_θ and ε_z are the radial, circumferential, and axial strains, respectively. ε_v is the volumetric strain. ε_1 and ε_3 are the major and minor principle strains, respectively. ε_{1e} is the elastic strain of the interface between the plastic and elastic regions. ε_1^p and ε_3^p are the major and minor plastic principal strains, respectively.

2.4 Strain-softening behaviour of the rock mass

A strain-softening material behaviour model proposed by Brown *et al.* (1983) is adopted for analysis in this study.

The idealized relationships of ε_1 and $\sigma'_1 - \sigma'_3$, ε_3, and ε_v used in this behaviour model are represented in Fig. 3. The strength reduction from the peak and the continued deformation at the residual region are both accompanied by plastic dilation. In Fig. 3, $\lambda\varepsilon_{1e}$ is the maximum principal strain component at the interface between the softening and residual regions. Therefore, the strain components (i.e., ε_1^p, ε_3^p, and ε_v^p) are the post-peak plastic strain increments.

The elastic volume increases when stresses are reduced. The evolution of the strength and deformation parameters (e.g., the dilation angle, cohesion, internal friction angle, elastic modulus, and Poisson's ratio) occur in the post-peak region, which is explicitly considered. h and H represent the gradients of the ε_3–ε_1 and ε_v–ε_1 curves, respectively,

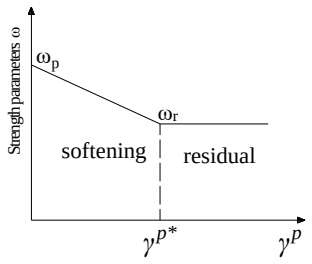

Fig. 4 Evolution of the strength parameter in the plastic region

corresponding to the post-peak condition. The strain components (i.e., ε_1^p, ε_3^p, and ε_v^p) are considered as the plastic strains. Experiments are required to determine the parameters (e.g., λ, f, h, F, and H) and their dependences on σ'_3.

2.5 Failure criterion

The yielding function in rock mass is expressed as follows:

$$\mathrm{F}\left(\sigma_1^{'},\sigma_3^{'},\gamma^{\mathrm{p}}\right)=\sigma_1^{'}-\sigma_3^{'}-\mathrm{H}\left(\sigma_3^{'},\gamma^{\mathrm{p}}\right) \tag{2a}$$

where, γ^p is the deviatoric plastic strain controlling the evolution of the strain-softening behaviour in the softening region, which can be expressed by the following equation (Alonso *et al.* 2003)

$$\gamma^p=\gamma_1^{\mathrm{p}}-\gamma_3^{\mathrm{p}} \tag{2b}$$

where, γ_1^p and γ_3^p are the major and minor deviatoric strains, respectively.

For the M-C failure criterion, H in Eq. (2a) becomes

$$H^{MC}\left(\sigma_3^{'},\gamma^p\right)=\left(N\left(\gamma^p\right)-1\right)\sigma_3^{'}+Y\left(\gamma^p\right) \tag{3}$$

where, N and Y are the strength parameters defined by the cohesion $c(\gamma^p)$ and internal friction angle ϕ (γ^p),

$$\begin{aligned} N\left(\gamma^p\right)&=\frac{1+\sin\phi\left(\gamma^p\right)}{1-\sin\phi\left(\gamma^p\right)}\\ Y\left(\gamma^p\right)&=\frac{2\mathrm{c}\left(\gamma^p\right)\cos\phi\left(\gamma^p\right)}{1-\sin\phi\left(\gamma^p\right)} \end{aligned} \tag{4}$$

In Eq. (2a), H can be expressed by Eq. (5) if the generalized H–B failure criterion is adopted.

$$\begin{aligned} &H^{HB}\left(\sigma_3^{'},\gamma^p\right)=\\ &\sigma_c\left(\gamma^p\right)\left(m\left(\gamma^p\right)\frac{\sigma_3^{'}}{\sigma_c\left(\gamma^p\right)}+s\left(\gamma^p\right)\right)^{a(\gamma)} \end{aligned} \tag{5}$$

where, σ_c is the uniaxial compressive strength of the rock mass and a, m, and s are the strength parameters of the generalized H–B failure criterion (Ogawa 1987).

2.6 Strength parameter evolution

The strength parameter reduction of the surrounding

rock presented by Lee and Pietruszczak (2008) can be expressed as follows

$$\omega\left(\gamma^p\right)=\begin{cases}\omega_p-\dfrac{\omega_p-\omega_r}{\gamma^p}\gamma^p, & 0<\gamma^p<\gamma^p\\ \omega_r, & \gamma^p\geq\gamma^p\end{cases} \tag{6}$$

where, ω represents one of the following strength parameters: ϕ, c, σ_c, m, s, a, and φ. γ^p. Subscripts p and r represent the peak and residual values, respectively.

2.7 Seepage force

This study adopts an effective method to define the seepage force. In the axisymmetric plane-strain problem, the seepage force F_r is the volume force

$$F_r=-\gamma_w i=\frac{dp_w}{dr}=-\gamma_w\frac{d(\xi H)}{dr}=\frac{\gamma_w\xi(h_a-h_0)}{r\ln\alpha} \tag{7}$$

where, α is a constant of the seepage force and α =30 is sufficient to satisfy engineering accuracy, I is the hydraulic gradient, ξ is the rock effective coefficient of the pore water pressure, γ_w is the unit weight of water, p_w is the pore water pressure, H is the water level fluctuation, r donates the radial distance from the centre of the opening, h_0 and h_a are respectively the waterhead on tunnel wall and infinity after excavation.

When taking into account of the seepage force, the Biot's effective stresses are adopted in the equilibrium differential equation. The stress equilibrium differential equation can be shown as follows,

$$\frac{d\sigma_r'}{dr}+\frac{\sigma_r'-\sigma_\theta'}{r}+F_r=0 \tag{8}$$

where, σ'_r and σ'_θ are the radial and circumferential effective stresses, respectively.

The stress and displacement in the elastic region can be expressed as follows (Bui *et al.* 2014),

$$\begin{aligned}\sigma_r'=&\sigma_0+\gamma_w\xi(h_a-h_0)+\frac{\gamma_w\xi(h_a-h_0)}{2(1-\nu)\ln\alpha}\ln\frac{r}{b}\\&+\frac{R^2}{R^2-b^2}\left(\frac{b^2}{r^2}-1\right)[\sigma_0+\gamma_w\xi(h_a-h_0)\\&-\sigma_R'+\frac{\gamma_w\xi(h_a-h_0)}{2(1-\nu)\ln\alpha}\ln\frac{R}{b}]\end{aligned} \tag{9}$$

$$\begin{aligned}\sigma_\theta'=&\sigma_0+\gamma_w\xi(h_a-h_0)\\&+\frac{\gamma_w\xi(h_a-h_0)}{2\ln\alpha}\left[\frac{\ln(r/b)}{1-\nu}+\frac{2\nu-1}{1-\nu}\right]\\&-\frac{R^2}{R^2-b^2}\left(\frac{b^2}{r^2}+1\right)[\sigma_0+\gamma_w\xi(h_a-h_0)\\&-\sigma_R'+\frac{\gamma_w\xi(h_a-h_0)}{2(1-\nu)\ln\alpha}\ln\frac{R}{b}]\end{aligned} \tag{10}$$

$$\sigma_z'=q \tag{11}$$

$$\begin{aligned}\frac{u}{r}=&\frac{1}{2G}\{(1-2\nu)\gamma_w\xi(h_a-h_0)\\&+(1-2\nu)\frac{\gamma_w\xi(h_a-h_0)}{2\ln\alpha}\left[\frac{\ln(r/b)}{1-\nu}-1\right]\\&-\frac{R^2}{R^2-b^2}\left(\frac{b^2}{r^2}+1-2\nu\right)[\sigma_0+\gamma_w\xi(h_a-h_0)\\&-\sigma_R'+\frac{\gamma_w\xi(h_a-h_0)}{2(1-\nu)\ln\alpha}\ln\frac{R}{b}]\}\end{aligned} \tag{12}$$

where, b is a relatively large constant, which represents infinity away from the tunnel wall.

2.8 Types of plastic zone around the tunnel

The plastic region occurs when the internal support pressure reaches a critical value. The plastic region can be divided into the softening and residual regions in strain-softening surrounding rock. So the softening radius R_s in Fig. 1 is used for dividing the softening and residual regions.

Previous theories have stated that the relationship of stress in the inner plastic region is $\sigma_z'>\sigma_\theta'>\sigma_r'$ (i.e., the out-of-plane stress is the major principal stress). σ_z' decreases and σ_θ' increases with decreasing internal pressure (p_{in}) until $\sigma_z'=\sigma_\theta'>\sigma_r'$ appears at a certain stage. The plastic radius of the circle opening between two regions with $\sigma_z'>\sigma_\theta'>\sigma_r'$ and $\sigma_z'=\sigma_\theta'>\sigma_r'$ is expressed by $\bar{R}$.

The second stage appears with $\sigma_\theta'>\sigma_z'>\sigma_r'$ (i.e., the out-of-plane stress is the intermediate principal stress). When the internal support pressure (p_{in}) continuously decreases, two states will appear with $\sigma_\theta'=\sigma_z'>\sigma_r'$ or $\sigma_\theta'>\sigma_z'=\sigma_r'$.

The third stage emerges with $\sigma_\theta'>\sigma_r'>\sigma_z'$ (i.e., the out-of-plane stress is the minor principal stress). Another stage corresponding to $\sigma_\theta'>\sigma_r'=\sigma_z'$ occurs as the internal support pressure (p_{in}) further decreases.

2.9 Internal supporting pressure in the critical state

The internal support pressure (p_{in}) in the critical state is related to σ'_z, σ'_θ, and σ'_r. σ'_θ is always larger than σ'_r according to the mechanical analysis. When the surrounding rock is in the elastic–plastic critical state, Eq. (10) becomes

$$\begin{aligned}\sigma_\theta'=&\frac{\gamma_w\xi(h_a-h_0)}{[2(1-\nu)\ln\alpha]}(2\nu-1)+p_{in}\\&-\frac{2b^2}{r_0^2-b^2}[\sigma_0-p_{in}+\gamma_w\xi(h_a-h_0)\\&+\frac{\gamma_w\xi(h_a-h_0)}{[2(1-\nu)\ln\alpha]}\ln\frac{r_0}{b}]\end{aligned} \tag{13}$$

(1) M–C failure criterion

When the out-of-plane stress along the tunnel axis is the major, intermediate or minor principal stresses, the

corresponding critical internal pressures (p_{c1}^{*} , p_{c2}^{*} and p_{c3}^{*}) can be respectively expressed by:

$$p_{c1}^{*}=\left(q-Y_p\right)/N_p \tag{14}$$

$$\begin{aligned}p_{c2}^{MC}=\{&\frac{\gamma_w\xi(h_a-h_0)}{2\ln\alpha}\frac{2\nu-1}{1-\nu}\\&-Y_p-\frac{2b^2}{r_0^2-b^2}\times[\sigma_0+\gamma_w\xi\left(h_a-h_0\right)\\&+\frac{\gamma_w\xi\left(h_a-h_0\right)}{2\left(1-\nu\right)\ln\alpha}\ln\frac{r_0}{b}]\}/(N_p-1-\frac{2b^2}{r_0^2-b^2})\end{aligned} \tag{15}$$

$$\begin{aligned}p_{c3}^{MC}=\{&\frac{\gamma_w\xi(h_a-h_0)}{2\ln\alpha}\frac{2\nu-1}{1-\nu}-N_pq\\&-Y_p-\frac{2b^2}{r_0^2-b^2}\times[\sigma_0+\gamma_w\xi\left(h_a-h_0\right)\\&+\frac{\gamma_w\xi\left(h_a-h_0\right)}{2\left(1-\nu\right)\ln\alpha}\ln\frac{r_0}{b}]\}/(-1-\frac{2b^2}{r_0^2-b^2})\end{aligned} \tag{16}$$

(2) Generalized H–B failure criterion

When the out-of-plane stress is the major, intermediate or minor principal stresses, the corresponding critical internal pressures (p_{c1}^{HB} , p_{c2}^{HB} and p_{c3}^{HB}) are expressed by the following equations:

$$q=p_{c1}^{HB}+\sigma_c(m_b\frac{p_{c1}^{HB}}{\sigma_c}+s)^a \tag{17}$$

$$\begin{aligned}&\frac{\gamma_w\xi(h_a-h_0)}{2\ln\alpha}\frac{2\nu-1}{1-\nu}\\&-\frac{2b^2}{r_0^2-b^2}[\sigma_0-p_{c2}^{HB}+\gamma_w\xi(h_a-h_0)\\&+\frac{\gamma_w\xi(h_a-h_0)}{2(1-\nu)\ln\alpha}\ln\frac{r_0}{b}]=\sigma_c(m_b\frac{p_{c2}^{HB}}{\sigma_c}+s)^a\end{aligned} \tag{18}$$

$$\begin{aligned}p_{c3}^{HB}=\{&\frac{\gamma_w\xi(h_a-h_0)}{2\ln\alpha}\frac{2\nu-1}{1-\nu}\\&-q-\sigma_c(m_b\frac{q}{\sigma_c}+s)^a\\&-\frac{2b^2}{r_0^2-b^2}\times[\sigma_0+\gamma_w\xi(h_a-h_0)\\&+\frac{\gamma_w\xi(h_a-h_0)}{2(1-\nu)\ln\alpha}\ln\frac{r_0}{b}]\}/(-1-\frac{2b^2}{r_0^2-b^2})\end{aligned} \tag{19}$$

When the out-of-plane stress is the intermediate principal stress, according to Eq. (18), $p_{in}=p_{c2}$ and $\sigma_r'\big|_{r=r_0}=p_{in}$, which is defined by

$$q_1=p_{c2} \tag{20}$$

The circumferential stress is determined by

$$\begin{aligned}\sigma_\theta'=&\frac{\gamma_w\xi\left(h_a-h_0\right)}{2\ln\alpha}\frac{2\nu-1}{1-\nu}+p_{c2}\\&-\frac{2b^2}{r_0^2-b^2}\times[\sigma_0-p_{c2}+\gamma_w\xi\left(h_a-h_0\right)\\&+\frac{\gamma_w\xi\left(h_a-h_0\right)}{2\left(1-\nu\right)\ln\alpha}\ln\frac{r_0}{b}]\end{aligned} \tag{21}$$

$$q_2=\sigma_\theta' \tag{22}$$

Since $q_2>q>q_1$, combining Eqs. (20)-(22), the out-of-plane stress can be obtained.

The radial stress (σ'_R) acting on the elastic–plastic interface is equal to p_{ci} (i.e., $\sigma_R'=\sigma_r'\left(R\right)=p_{ci}$), when the plastic region is formed.

2.10 Increments of strain and stress

The plastic region is divided into n concentric annuli. The ith annulus is bounded by two circles of normalized radii, $\rho_{(i-1)}=r_{(i-1)}/R$ and $\rho_{(i)}=r_{(i)}/R$.

$\rho_{(0)}=1$ on the outer boundary of the plastic region (elastic-plastic interface). The stress and strain components can be written as

$$\begin{Bmatrix}\sigma_{r(0)}'\\\sigma_{\theta(0)}'\\\sigma_{z(0)}'\end{Bmatrix}=\begin{Bmatrix}\sigma_R'\\\sigma_\theta'\\q\end{Bmatrix} \tag{23}$$

$$\begin{Bmatrix}\varepsilon_r\\\varepsilon_\theta\end{Bmatrix}=\begin{Bmatrix}du/dr\\u/r\end{Bmatrix} \tag{24}$$

Combining Eqs. (12) and (24), the original strains can be expressed as follows:

$$\begin{cases}\begin{aligned}\varepsilon_{r(0)}=&\frac{1}{2G}\{\sigma_R'-\sigma_0-2\nu\gamma_w\xi(h_a-h_0)\\&-\frac{\nu\gamma_w\xi(h_a-h_0)}{2\left(1-\nu\right)\ln\alpha}[2\ln\left(R/b\right)-\left(1-2\nu\right)]\\&+\frac{2\nu\left(R/b\right)^2}{\left(R/b\right)^2-1^2}[\sigma_0+\gamma_w\xi(h_a-h_0)\\&-\sigma_R'+\frac{\gamma_w\xi(h_a-h_0)}{2\left(1-\nu\right)\ln\alpha}\ln\frac{R}{b}]\}\\\varepsilon_{\theta(0)}=&\frac{1}{2G}\{\sigma_0-\sigma_R'+2\left(1-\nu\right)\gamma_w\xi\left(h_a-h_0\right)\\&+\frac{\gamma_w\xi(h_a-h_0)}{2\ln\alpha}\left[2\ln\left(R/b\right)-\left(1-2\nu\right)\right]\\&-\frac{2\left(R/b\right)^2\left(1-\nu\right)}{\left(R/b\right)^2-1^2}[\sigma_0-\sigma_R'\\&+\gamma_w\xi\left(h_a-h_0\right)+\frac{\gamma_w\xi\left(h_a-h_0\right)}{2\left(1-\nu\right)\ln\alpha}\ln\frac{R}{b}]\}\\\varepsilon_{z(0)}=&0\end{aligned}\end{cases} \tag{25}$$

The internal support pressure is assumed to decrease monotonically from σ'_R to p_{in} with step of $\Delta\sigma'_r$ in Eq. (26). This numerical method is proposed by Park *et al.* (2008) and Lee *et al.* (2008) based on finite difference principle.

The radial stress increment can be determined by

$$\Delta\sigma_{\mathrm{r}}^{'}=\frac{\left(\mathrm{p_{in}}-\sigma_{\mathrm{R}}^{'}\right)}{\mathrm{n}} \tag{26}$$

The radial stress can be calculated by,

$$\sigma_{\mathrm{r(i)}}^{'}=\sigma_{\mathrm{r(i-1)}}^{'}+\Delta\sigma_{\mathrm{r}}^{'} \tag{27}$$

The stress and plastic strain increments are expressed as,

$$\Delta\sigma_{\mathrm{z(i)}}^{'}=\sigma_{\mathrm{z(i)}}^{'}-\sigma_{\mathrm{z(i-1)}}^{'} \tag{28}$$

$$\Delta\sigma_{\theta\mathrm{(i)}}^{'}=\sigma_{\theta\mathrm{(i)}}^{'}-\sigma_{\theta\mathrm{(i-1)}}^{'} \tag{29}$$

$$\Delta\varepsilon_{\mathrm{(i)}}^{\mathrm{p}}=\varepsilon_{\mathrm{(i)}}^{\mathrm{p}}-\varepsilon_{\mathrm{(i-1)}}^{\mathrm{p}} \tag{30}$$

Strain at any point in the plastic region is composed of elastic and plastic parts. Therefore, the strain of the ith annulus at any point is equal to the sum of $\varepsilon_{\mathrm{(i-1)}}$ and the elastic and plastic increments: $\varepsilon_{\mathrm{(i)}}=\varepsilon_{\mathrm{(i-1)}}+\Delta\varepsilon^{\mathrm{e}}+\Delta\varepsilon^{\mathrm{p}}$.

The plastic shear strain is then obtained by

$$\gamma_{\mathrm{(i)}}^{\mathrm{p}}=\gamma_{\mathrm{(i-1)}}^{\mathrm{p}}+\left(\Delta\varepsilon_{1\mathrm{(i)}}^{\mathrm{p}}-\Delta\varepsilon_{3\mathrm{(i)}}^{\mathrm{p}}\right) \tag{31}$$

where, ε_1 and ε_3 are the major and minor plastic strains, respectively.

3. Governing equation (control equation) and solutions

3.1 σ_z is the major principal stress

(1) Failure criterion

When the out-of-plane stress is the major principal stress (i.e., $\sigma_{\mathrm{z}}^{'}>\sigma_{\theta}^{'}>\sigma_{\mathrm{r}}^{'}$). The failure criteria are given by defining $\sigma_1^{'}=\sigma_{\mathrm{z}}^{'}$ and $\sigma_3^{'}=\sigma_{\mathrm{r}}^{'}$ in Eq. (2a).

(2) Initial stress and strain

According to Eqs. (13) and (23), the initial stress is represented as

$$\sigma_{\mathrm{r(0)}}^{'}=\mathrm{p_{c1}} \tag{32}$$

$$\begin{aligned}\sigma_{\theta\mathrm{(0)}}^{'}=\sigma_{\theta}^{'}=&\frac{\gamma_{\mathrm{w}}\xi\left(\mathrm{h_a}-\mathrm{h_0}\right)}{2\ln\alpha}\frac{2\nu-1}{1-\nu}+\mathrm{p_{c1}}\\&-\frac{2\mathrm{b}^2}{\mathrm{r_0^2}-\mathrm{b}^2}[\sigma_0-\mathrm{p_{c1}}+\gamma_{\mathrm{w}}\xi\left(\mathrm{h_a}-\mathrm{h_0}\right)\\&+\frac{\gamma_{\mathrm{w}}\xi\left(\mathrm{h_a}-\mathrm{h_0}\right)}{2\left(1-\nu\right)\ln\alpha}\ln\frac{\mathrm{r_0}}{\mathrm{b}}]\end{aligned} \tag{33}$$

In Eqs. (32) and (33), $\mathrm{p_{c1}}=\mathrm{p_{c1}^{MC}}$ for the M–C failure criterion, and $\mathrm{p_{c1}}=\mathrm{p_{c1}^{HB}}$ for the generalized H–B failure criterion, derived using Eqs. (14) and (17), respectively.

Accordingly,

$$\sigma_{\mathrm{z(0)}}^{'}=\mathrm{q} \tag{34}$$

The corresponding initial strain is presented in Eq. (25).

(3) Radius

The strain compatibility equation is given by

$$\frac{\mathrm{d}\varepsilon_{\theta}}{\mathrm{dr}}+\frac{\varepsilon_{\theta}-\varepsilon_{\mathrm{r}}}{\mathrm{r}}=0 \tag{35}$$

The following equation can be obtained in terms of strain compatibility equation, non-associate flow rule ($\varepsilon_r^p+\beta\varepsilon_z^p=0$) and Hooke's law:

$$\begin{aligned}\sigma_{\theta\mathrm{(i)}}^{'}=&[(\frac{\overline{\rho_{\mathrm{(i)}}}}{\Delta\rho_{\mathrm{(i)}}}-\frac{\left(1+\nu+\nu\beta\right)}{2})\sigma_{\theta\mathrm{(i-1)}}^{'}\\&+\nu\frac{\overline{\rho_{\mathrm{(i)}}}}{\Delta\rho_{\mathrm{(i)}}}(\Delta\sigma_{\mathrm{r(i)}}^{'}+\Delta\sigma_{\mathrm{z(i)}}^{'})+\left(1+\nu-\nu\beta\right)\overline{\sigma_{\mathrm{r(i)}}^{'}}\\&+\beta\overline{\sigma_{\mathrm{z(i)}}^{'}}-\beta\left(\mathrm{q}-2\nu\sigma_0\right)]/(\frac{\overline{\rho_{\mathrm{(i)}}}}{\Delta\rho_{\mathrm{(i)}}}+\frac{\left(1+\nu+\nu\beta\right)}{2})\end{aligned} \tag{36}$$

where, $\overline{\sigma_{\mathrm{(i)}}^{'}}=(\sigma_{\mathrm{(i)}}^{'}+\sigma_{\mathrm{(i-1)}}^{'})/2$ and $\overline{\rho_{\mathrm{(i)}}}=(\rho_{\mathrm{(i)}}+\rho_{\mathrm{(i-1)}})/2$.

The equilibrium differential equation is expressed as follows considering the seepage force:

$$\frac{\mathrm{d}\sigma_{\mathrm{r}}^{'}}{\mathrm{d}\rho}+\frac{\sigma_{\mathrm{r}}^{'}-\sigma_{\theta}^{'}}{\rho}+\frac{\gamma_{\mathrm{w}}\xi\left(\mathrm{h_a}-\mathrm{h_0}\right)}{\rho\ln\alpha}=0 \tag{37}$$

We solve Eq. (37) as:

$$\overline{\rho_{\mathrm{(i)}}}(\frac{\Delta\sigma_{\mathrm{r(i)}}^{'}}{\Delta\rho_{\mathrm{(i)}}}+\frac{\gamma_{\mathrm{w}}\xi\left(\mathrm{h_a}-\mathrm{h_0}\right)}{\rho\ln\alpha})=\overline{\sigma_{\theta\mathrm{(i)}}^{'}}-\overline{\sigma_{\mathrm{r(i)}}^{'}} \tag{38}$$

The following equation is obtained by substituting Eq. (36) into Eq. (38):

$$\begin{aligned}&2\Delta\sigma_{\mathrm{r(i)}}^{'}(\frac{\overline{\rho_{(\,)}}}{\Delta\rho_{\mathrm{(i)}}})^2-[\nu\Delta\sigma_{\mathrm{r(i)}}^{'}+\nu\Delta\sigma_{\mathrm{z(i)}}^{'}\\&+2\sigma_{\theta\mathrm{(i-1)}}^{'}-2\overline{\sigma_{\mathrm{r(i)}}^{'}}-\left(1+\nu+\nu\beta\right)\Delta\sigma_{\mathrm{r(i)}}^{'}\\&-2\frac{\gamma_{\mathrm{w}}\xi\left(\mathrm{h_a}-\mathrm{h_0}\right)}{\ln\alpha}]\frac{\overline{\rho_{\mathrm{(i)}}}}{\Delta\rho_{\mathrm{(i)}}}\\&-[\beta\overline{\sigma_{\mathrm{z(i)}}^{'}}-\beta\left(\mathrm{q}-2\nu\sigma_0-\mathrm{Y_{i-1}}\right)-2\nu\beta\overline{\sigma_{\mathrm{r(i)}}^{'}}\\&-\left(1+\nu+\nu\beta\right)\frac{\gamma_{\mathrm{w}}\xi\left(\mathrm{h_a}-\mathrm{h_0}\right)}{\ln\alpha}]=0\end{aligned} \tag{39}$$

Then $\rho_{\mathrm{(i)}}$ can be solved using Eq. (39). $\sigma'_{\theta\mathrm{(i)}}$ can also be obtained by substituting the calculated $\rho_{\mathrm{(i)}}$ into Eq. (36). $\sigma'_{z\mathrm{(i)}}$ is then given by the M–C or the generalized H–B failure criterion.

(4) Displacement

We have $\varepsilon_{\theta\mathrm{(i)}}^{\mathrm{p}}=0$ and $\varepsilon_{\mathrm{z(i)}}=0$, in addition, $\Delta\varepsilon_{\mathrm{z(i)}}^{\mathrm{p}}=-\Delta\varepsilon_{\mathrm{z(i)}}^{\mathrm{e}}$. The following equation is obtained using the non-associate flow rule:

$$\sigma_{\mathrm{r(0)}}^{'}=\mathrm{p_{c1}} \tag{40}$$

where, $\beta_{\mathrm{(i-1)}}=(1+\sin\varphi_{\mathrm{(i-1)}})/(1-\sin\varphi_{\mathrm{(i-1)}})$ and φ is the dilation angle.

In terms of $\rho(\mathrm{i})=\mathrm{r(i)}/\mathrm{R}$, the plastic radius results is

shown as,

$$R = r_0 / \rho_n \tag{41}$$

The following formula is obtained because of ε_θ=u/r:

$$U_{(i)} = \varepsilon_{\theta(i)} \rho_{(i)} \tag{42}$$

The displacement of each concentric circle can be determined using Eq. (43) as following:

$$u_{(i)} = U_{(i)} R \tag{43}$$

The softening region occurs with $\sigma_\theta^{'} = \sigma_z^{'} > \sigma_r^{'}$ when the internal support pressure further decreases. In this case, the solutions of the stress, strain, and plastic radius can also be determined using similar solving methods as the condition under which the out-of-plane stress is the intermediate principal stress and $\sigma_\theta^{'} = \sigma_z^{'} > \sigma_r^{'}$. This method will be presented in the following section.

3.2 σ_z is the intermediate principal stress

(1) Failure criterion

The failure criteria can be described by denoting $\sigma_1^{'} = \sigma_\theta^{'}$ and $\sigma_3^{'} = \sigma_r^{'}$ in Eq. (2a) because the out-of-plane stress is the intermediate principal stress in this case.

(2) Initial stress and strain

According to Eq. (23), the radial stress leads to

$$\sigma_{r(0)}^{'} = p_{c2} \tag{44}$$

In Eq. (44), $p_{c2} = p_{c2}^{MC}$ and $p_{c2} = p_{c2}^{HB}$ for the M–C and the generalized H–B failure criterion obtained using Eqs. (15) and (18), respectively.

Combining Eqs. (21) and (24), the circumferential initial stress is solved using Eq. (21).

Substituting Eq. (21) into Eq. (25), the initial strain in the critical state is obtained.

(3) Stress increment

The circumferential stress can be obtained using the failure criterion. The axial in situ stress is given by Eq. (45):

$$\sigma_{z(i)}^{'} = \nu\left(\sigma_{\theta(i)}^{'} + \sigma_{r(i)}^{'}\right) - 2\nu\sigma_0 + q \tag{45}$$

(4) Radius of each concentric circle

Solving Eq. (38), the control equation of the radius for each concentric circle is given by

$$\frac{\sigma_{r(i)}^{'} - \sigma_{r(i-1)}^{'}}{\rho_{(i)} - \rho_{(i-1)}} - \frac{2\overline{H(\sigma_{r(i)}^{'}, \eta)} - 2\gamma_w \xi\left(h_a - h_0\right)/\ln\alpha}{\rho_{(i)} + \rho_{(i-1)}} = 0 \tag{46}$$

where, $H(\sigma_{r(i)}^{'}, \eta)$ is the coefficient in Eqs. (3) and (5).

Solving Eq. (46), the radius of each concentric circle is determined by Eq. (47) as follows:

$$\begin{aligned}\rho_{(i)} &= \rho_{(i-1)} \\ &\times [2\overline{H(\sigma_{r(i)}^{'}, \eta)} - 2\gamma_w \xi\left(h_a - h_0\right)/\ln\alpha + \Delta\sigma_r^{'}] \\ &/ [2\overline{H(\sigma_{r(i)}^{'}, \eta)} - 2\gamma_w \xi\left(h_a - h_0\right)/\ln\alpha - \Delta\sigma_r^{'}]\end{aligned} \tag{47}$$

(5) Plastic radius and displacement

The following equation is obtained according to Eq. (35):

$$\frac{d\varepsilon_\theta^p}{d\rho} + \frac{\varepsilon_\theta^p - \varepsilon_r^p}{\rho} = -\frac{d\varepsilon_\theta^e}{d\rho} - \frac{\varepsilon_\theta^e - \varepsilon_r^e}{\rho} \tag{48}$$

Subsequently, Eq. (48) can be rewritten as

$$\frac{d\varepsilon_\theta^p}{d\rho} + \frac{\varepsilon_\theta^p - \varepsilon_r^p}{\rho} = -\frac{d\varepsilon_\theta^e}{d\rho} - \frac{1+\nu}{E}\frac{H\left(\sigma_r^{'}, \gamma^p\right)}{\rho} \tag{49}$$

The following equation is obtained considering the non-associate flow rule and boundary condition:

$$\begin{cases}\varepsilon_r^p + \beta\varepsilon_\theta^p = 0 \\ \varepsilon_z^p = 0\end{cases} \tag{50}$$

Eq. (51) is derived using Eqs. (49) and (50):

$$\begin{aligned}\Delta\varepsilon_{\theta(i)}^p = (&-\frac{\Delta\varepsilon_{\theta(i)}^e}{\Delta\rho_{(i)}} - \frac{1+\nu}{E}\frac{\overline{H(\sigma_{r(i)}^{'}, \eta_{(i-1)})}}{\overline{\Delta\rho_{(i)}}} \\ &- \frac{\varepsilon_{\theta(i-1)}^p - \varepsilon_{r(i-1)}^p}{\overline{\Delta\rho_{(i)}}}) / (\frac{1}{\Delta\rho_{(i)}} + \frac{(1+\beta_{i-1})}{\overline{\Delta\rho_{(i)}}})\end{aligned} \tag{51}$$

The following equation is subsequently obtained:

$$\Delta\varepsilon_{r(i)}^p = -\beta_{(i-1)}\Delta\varepsilon_{\theta(i)}^p \tag{52}$$

The plastic radius and the displacement are obtained using Eqs. (41) and (43), respectively.

Eqs. (50)-(52) are used to calculate the plastic strains when the stress state is $\sigma_\theta^{'} > \sigma_z^{'} > \sigma_r^{'}$ in the plastic region. The following paragraphs describe the plastic strains when the stress state is $\sigma_\theta^{'} = \sigma_z^{'} > \sigma_r^{'}$ or $\sigma_\theta^{'} > \sigma_z^{'} = \sigma_r^{'}$ in the plastic region.

The plastic region appears with $\sigma_\theta^{'} = \sigma_z^{'} > \sigma_r^{'}$ when the out-of-plane stress (q) is sufficiently large and the internal support pressure (p_{in}) is sufficiently small. At this point, the radial stress can be obtained using Eq. (27). Moreover, the circumferential and axial stresses are given by the M–C or the generalized H-B failure criterion. The radius of each concentric circle is determined by Eq. (47).

From Eq. (49), the non-associate flow rule ($\varepsilon_r^p + \beta\varepsilon_\theta^p + \beta\varepsilon_z^p = 0$), and the boundary condition ($\varepsilon_z^p = 0$), Eq. (53) is derived as follows:

$$\begin{aligned}\Delta\varepsilon_{\theta(i)}^p = (&-\frac{\Delta\varepsilon_{\theta(i)}^e}{\Delta\rho_{(i)}} - \frac{1+\nu}{E}\frac{\overline{H(\sigma_{r(i)}^{'}, \eta_{(i-1)})}}{\overline{\Delta\rho_{(i)}}} \\ &- \frac{\varepsilon_{\theta(i-1)}^p - \varepsilon_{r(i-1)}^p}{\overline{\Delta\rho_{(i)}}} + \frac{\beta\Delta\varepsilon_{z(i)}^e}{\overline{\Delta\rho_{(i)}}}) \\ &/ (\frac{1}{\Delta\rho_{(i)}} + \frac{(1+\beta_{i-1})}{\overline{\Delta\rho_{(i)}}})\end{aligned} \tag{53}$$

The plastic radius and the displacement can be determined using Eqs. (41) and (43), respectively. $\Delta\varepsilon^{\mathrm{p}}_{\theta(\mathrm{i})}$ can be solved using Eq. (53).

The plastic region occurs with $\sigma'_\theta > \sigma'_\mathrm{r} = \sigma'_\mathrm{z}$ when the out-of-plane stress (q) and the internal support pressure (p_{in}) continuously decrease. The radial stress is obtained using Eq. (27), and the circumferential stress is determined by the M–C or the generalized H–B failure criterion. The radius of each concentric circle is given by Eq. (47).

The following equation is obtained based on Eq. (48), the non-associate flow rule ($\varepsilon^{\mathrm{p}}_\mathrm{r} + \beta\varepsilon^{\mathrm{p}}_\theta + \varepsilon^{\mathrm{p}}_\mathrm{z} = 0$) and the boundary condition ($\varepsilon^{\mathrm{p}}_\mathrm{r} = 0$):

$$\begin{aligned}\Delta\varepsilon^{\mathrm{p}}_{\theta(\mathrm{i})} = &\Big(-\frac{\Delta\varepsilon^{\mathrm{e}}_{\theta(\mathrm{i})}}{\Delta\rho_{(\mathrm{i})}} - \frac{1+\nu}{\mathrm{E}}\frac{\mathrm{H}\left(\overline{\sigma'_{\mathrm{r}(\mathrm{i})}}, \eta_{(\mathrm{i}-1)}\right)}{\overline{\Delta\rho_{(\mathrm{i})}}} \\ &- \frac{\varepsilon^{\mathrm{p}}_{\theta(\mathrm{i}-1)} - \varepsilon^{\mathrm{p}}_{\mathrm{r}(\mathrm{i}-1)}}{\overline{\Delta\rho_{(\mathrm{i})}}} + \frac{\Delta\varepsilon^{\mathrm{e}}_{\mathrm{z}(\mathrm{i})}}{\overline{\Delta\rho_{(\mathrm{i})}}}\Big) \\ &/\Big(\frac{1}{\Delta\rho_{(\mathrm{i})}} + \frac{(1+\beta_{\mathrm{i}-1})}{\overline{\Delta\rho_{(\mathrm{i})}}}\Big)\end{aligned} \tag{54}$$

$\Delta\varepsilon^{\mathrm{p}}_{\theta(\mathrm{i})}$ can be determined using Eq. (54). The displacement and the plastic radius are similar to those in Eqs. (41) and (43), respectively.

3.3 σ_z is the minor principal stress

(1) Failure criterion

The failure criterion is given by defining $\sigma'_1 = \sigma'_\theta$ and $\sigma'_3 = \sigma'_\mathrm{z}$ in Eq. (2a) because the out-of-plane stress is the minor principal stress.

The following formula is derived according to Eq. (48), the non-associate flow rule ($\varepsilon^{\mathrm{p}}_\mathrm{z} + \beta\varepsilon^{\mathrm{p}}_\theta = 0$), the boundary condition ($\varepsilon^{\mathrm{p}}_\mathrm{r} = 0$) and Hooke's law:

$$\begin{aligned}&\mathrm{r}\Big[\Big(1-\frac{\nu}{\beta}\Big)\frac{\mathrm{d}\sigma'_\theta}{\mathrm{d}r} - \nu\Big(1+\frac{1}{\beta}\Big)\frac{\mathrm{d}\sigma'_\mathrm{r}}{\mathrm{d}r} + \Big(\frac{1}{\beta}-\nu\Big)\frac{\mathrm{d}\sigma'_\mathrm{z}}{\mathrm{d}r}\Big] \\ &= \Big(\frac{\nu}{\beta}-1-\nu\Big)\sigma'_\theta + \Big(1+\nu+\frac{\nu}{\beta}\Big)\sigma'_\mathrm{r} \\ &\quad -\frac{1}{\beta}\sigma'_\mathrm{z} + \frac{1}{\beta}(\mathrm{q}-2\nu\sigma_0)\end{aligned} \tag{55}$$

The following equation is obtained by solving Eq. (55):

$$\begin{aligned}&\frac{\overline{\rho_{(\mathrm{i})}}}{\Delta\rho_{(\mathrm{i})}}\Big[\Big(1-\frac{\nu}{\beta}\Big)\sigma'_{\theta(\mathrm{i})} - \Big(1-\frac{\nu}{\beta}\Big)\sigma'_{\theta(\mathrm{i}-1)} \\ &-\nu\Big(1+\frac{1}{\beta}\Big)\Delta\sigma'_{\mathrm{r}(\mathrm{i})} + \Big(\frac{1}{\beta}-\nu\Big)\sigma'_{\mathrm{z}(\mathrm{i})} \\ &-\Big(\frac{1}{\beta}-\nu\Big)\sigma'_{\mathrm{z}(\mathrm{i}-1)}\Big] \\ &= \Big(\frac{\nu}{2\beta}-\frac{1+\nu}{2}\Big)\sigma'_{\theta(\mathrm{i})} + \Big(\frac{\nu}{2\beta}-\frac{1+\nu}{2}\Big)\sigma'_{\theta(\mathrm{i}-1)} \\ &+\Big(1+\nu+\frac{\nu}{\beta}\Big)\overline{\sigma'_{\mathrm{r}(\mathrm{i})}} - \frac{1}{2\beta}\sigma'_{\mathrm{z}(\mathrm{i})} \\ &-\frac{1}{2\beta}\sigma'_{\mathrm{z}(\mathrm{i}-1)} + \frac{1}{\beta}(\mathrm{q}-2\nu\sigma_0)\end{aligned} \tag{56}$$

(2) M–C failure criterion

Substituting the M–C failure criterion $\sigma'_\theta = \mathrm{N}\sigma'_\mathrm{z} + \mathrm{Y}$ into Eq. (56), we obtain

$$\begin{aligned}\sigma'_{\mathrm{z}(\mathrm{i})} = &\{-[(1-\frac{\nu}{\beta})\mathrm{Y}_\mathrm{r} - (1-\frac{\nu}{\beta})\sigma'_{\theta(\mathrm{i}-1)} - \\ &\nu(1+\frac{1}{\beta})\Delta\sigma'_{\mathrm{r}(\mathrm{i})} - (\frac{1}{\beta}-\nu)\sigma'_{\mathrm{z}(\mathrm{i}-1)}]\frac{\overline{\rho_{(\mathrm{i})}}}{\Delta\rho_{(\mathrm{i})}} + \\ &[(\frac{\nu}{2\beta}-\frac{1+\nu}{2})\mathrm{Y}_\mathrm{r} + (\frac{\nu}{2\beta}-\frac{1+\nu}{2})\sigma'_{\theta(\mathrm{i}-1)} + \\ &(1+\nu+\frac{\nu}{\beta})\overline{\sigma'_{\mathrm{r}(\mathrm{i})}} - \frac{1}{2\beta}\sigma'_{\mathrm{z}(\mathrm{i}-1)} \\ &+\frac{1}{\beta}(\mathrm{q}-2\nu\sigma_0)]\}/[(\alpha_\mathrm{r} - \frac{\alpha_\mathrm{r}\nu}{\beta} + \frac{1}{\beta} - \nu)\frac{\overline{\rho_{(\mathrm{i})}}}{\Delta\rho_{(\mathrm{i})}} \\ &-\alpha_\mathrm{r}(\frac{\nu}{2\beta}-\frac{1+\nu}{2}) + \frac{1}{2\beta}]\end{aligned} \tag{57}$$

We derive the following by substituting Eq. (59) into the M–C failure criterion:

$$\begin{aligned}\sigma'_{\theta(\mathrm{i})} &= \mathrm{N}_{(\mathrm{i}-1)}\sigma'_{\mathrm{z}(\mathrm{i})} + \mathrm{Y}_{(\mathrm{i}-1)} \\ &= \mathrm{N}_{(\mathrm{i}-1)}\{-[(1-\frac{\nu}{\beta})\mathrm{Y}_\mathrm{r} - (1-\frac{\nu}{\beta})\sigma'_{\theta(\mathrm{i}-1)} - \\ &\quad \nu(1+\frac{1}{\beta})\Delta\sigma'_{\mathrm{r}(\mathrm{i})} - (\frac{1}{\beta}-\nu)\sigma'_{\mathrm{z}(\mathrm{i}-1)}]\frac{\overline{\rho_{(\mathrm{i})}}}{\Delta\rho_{(\mathrm{i})}} + \\ &\quad [(\frac{\nu}{2\beta}-\frac{1+\nu}{2})\mathrm{Y}_\mathrm{r} + (\frac{\nu}{2\beta}-\frac{1+\nu}{2})\sigma'_{\theta(\mathrm{i}-1)} + \\ &\quad (1+\nu+\frac{\nu}{\beta})\overline{\sigma'_{\mathrm{r}(\mathrm{i})}} - \frac{1}{2\beta}\sigma'_{\mathrm{z}(\mathrm{i}-1)} + \\ &\quad \frac{1}{\beta}(\mathrm{q}-2\nu\sigma_0)]\}/ \\ &\quad [(\mathrm{N}_\mathrm{r} - \frac{\alpha_\mathrm{r}\nu}{\beta} + \frac{1}{\beta} - \nu)\frac{\overline{\rho_{(\mathrm{i})}}}{\Delta\rho_{(\mathrm{i})}} \\ &\quad -\mathrm{N}_\mathrm{r}(\frac{\nu}{2\beta}-\frac{1+\nu}{2}) + \frac{1}{2\beta}] + \mathrm{Y}_{(\mathrm{i}-1)}\end{aligned} \tag{58}$$

The following equation is derived by combining Eqs. (38) and (58):

$$\begin{aligned}&2(\mathrm{N}_\mathrm{r} - \frac{\mathrm{N}_\mathrm{r}\nu}{\beta} + \frac{1}{\beta} - \nu)\Delta\sigma'_{\mathrm{r}(\mathrm{i})}(\frac{\overline{\rho_{(\mathrm{i})}}}{\Delta\rho_{(\mathrm{i})}})^2 \\ &= [-\mathrm{N}_{(\mathrm{i}-1)}(1-\frac{\nu}{\beta})(\mathrm{Y}_\mathrm{r} - \sigma'_{\theta(\mathrm{i}-1)}) + \\ &\quad \mathrm{N}_{(\mathrm{i}-1)}\nu(1+\frac{1}{\beta})\Delta\sigma'_{\mathrm{r}(\mathrm{i})} + \mathrm{N}_{(\mathrm{i}-1)}(\frac{1}{\beta}-\nu)\sigma'_{\mathrm{z}(\mathrm{i}-1)} + \\ &\quad (\mathrm{N}_\mathrm{r} - \frac{\mathrm{N}_\mathrm{r}\nu}{\beta} + \frac{1}{\beta} - \nu)(\mathrm{Y}_{(\mathrm{i}-1)} + \sigma'_{\theta(\mathrm{i}-1)} - 2\overline{\sigma'_{\mathrm{r}(\mathrm{i})}} - \\ &\quad 2\frac{\gamma_\mathrm{w}\xi(\mathrm{h_a} - \mathrm{h}_0)}{\ln\alpha}) + \\ &\quad (\frac{\mathrm{N}_\mathrm{r}\nu}{\beta} - \mathrm{N}_\mathrm{r} - \mathrm{N}_\mathrm{r}\nu - \frac{1}{\beta})\Delta\sigma'_{\mathrm{r}(\mathrm{i})}]\frac{\overline{\rho_{(\mathrm{i})}}}{\Delta\rho_{(\mathrm{i})}} + \\ &\quad [\mathrm{N}_{(\mathrm{i}-1)}(\frac{\nu}{2\beta}-\frac{1+\nu}{2})(\mathrm{Y}_\mathrm{r} + \sigma'_{\theta(\mathrm{i}-1)}) - \frac{\mathrm{N}_{(\mathrm{i}-1)}}{2\beta}\sigma'_{\mathrm{z}(\mathrm{i}-1)} \\ &\quad +\mathrm{N}_{(\mathrm{i}-1)}(1+\nu+\frac{\nu}{\beta})\overline{\sigma'_{\mathrm{r}(\mathrm{i})}} + \frac{\mathrm{N}_{(\mathrm{i}-1)}}{\beta}(\mathrm{q}-2\nu\sigma_0) - \\ &\quad (\frac{\mathrm{N}_\mathrm{r}\nu}{2\beta} - \frac{\mathrm{N}_\mathrm{r} + \mathrm{N}_\mathrm{r}\nu}{2} - \frac{1}{2\beta})(\mathrm{Y}_{(\mathrm{i}-1)} + \sigma'_{\theta(\mathrm{i}-1)} - \\ &\quad 2\overline{\sigma'_{\mathrm{r}(\mathrm{i})}} - 2\frac{\gamma_\mathrm{w}\xi(\mathrm{h_a} - \mathrm{h}_0)}{\ln\alpha})]\end{aligned} \tag{59}$$

where, $\rho_{(\mathrm{i})}$ is given by Eq. (59) using the iterative method. $\sigma'_{\mathrm{z}(\mathrm{i})}$ and $\sigma'_{\theta(\mathrm{i})}$ are solved using Eqs. (57) and (58),

respectively.

(3) Generalized H–B failure criterion

The generalized H–B failure criterion is given by

$$\sigma'_{\theta(i)}=\sigma'_{z(i)}+\sigma_{c(i-1)}\left(m_{(i-1)}\frac{\sigma'_{z(i)}}{\sigma_{c(i-1)}}+s_{(i-1)}\right)^{a}. \tag{60}$$

The following equation is obtained according to Eq. (38):

$$\begin{aligned}\rho_{(i)}=&\rho_{(i-1)}\times\\&[2\left(\overline{\sigma'_{\theta(i)}}-\overline{\sigma'_{r(i)}}-\gamma_w\xi\left(h_a-h_0\right)/\ln\alpha\right)+\Delta\sigma'_{r(i)}]/\\&2\left(\overline{\sigma'_{\theta(i)}}-\overline{\sigma'_{r(i)}}-\gamma_w\xi\left(h_a-h_0\right)/\ln\alpha\right)-\Delta\sigma'_{r(i)}\end{aligned} \tag{61}$$

$\sigma'_{z(i)}$, $\sigma'_{\theta(i)}$, and $\rho_{(i)}$ are then determined by Eqs. (56), (60), and (61), respectively.

The plastic radius and displacement are obtained using Eqs. (41) and (43), respectively.

The plastic region with $\sigma'_\theta>\sigma'_r=\sigma'_z$ occurs in the softening region when the internal support pressure (p_{in}) is sufficiently small. The solving methods of stress, strain, and displacement are similar to the condition under which the out-of-plane stress is the intermediate principal stress with $\sigma'_\theta>\sigma'_r=\sigma'_z$.

4. Verification

To confirm the validity and accuracy of the proposed solution, the results of the presented approach for elastic–brittle–plastic, elasto–plastic and strain-softening models are compared with the results of numerical simulation and those of Wang *et al.* (2012). The derived formulations are converted into computer code, and a set of rock parameters

Table 1 Results of plastic radius and displacement (The results of Wang *et al.* (2012) are enclosed in parentheses)

q (MPa)	Dilation angle	R/r_0	$2uG/(r_0\sigma_0)$
60	ebp (φ =7.5°)	1.88 (1.88)	5.63 (5.60)
	ebp (φ =19.5°)	1.88 (1.88)	9.33 (9.27)
	ep (φ =7.5°)	1.31 (1.31)	1.83 (1.82)
	ep (φ =19.5°)	1.31 (1.31)	2.25 (2.24)
54.22	ebp (φ =7.5°)	1.82 (1.82)	5.21(5.19)
	ebp (φ =19.5°)	1.82 (1.82)	8.42 (8.38)
	ep (φ =7.5°)	1.29 (1.29)	1.78 (1.78)
	ep (φ =19.5°)	1.29 (1.29)	2.16 (2.15)
30.00	ebp (φ =7.5°)	1.82 (1.82)	4.54 (4.52)
	ebp (φ =19.5°)	1.82 (1.82)	6.95 (6.90)
	ep (φ =7.5°)	1.29 (1.29)	1.65 (1.64)
	ep (φ =19.5°)	1.29 (1.29)	1.91 (1.91)
13.20	ebp (φ =7.5°)	1.82 (1.82)	4.35 (4.33)
	ebp (φ =19.5°)	1.82 (1.82)	6.58 (6.53)
	ep (φ =7.5°)	1.29 (1.29)	1.63 (1.62)
	ep (φ =19.5°)	1.29 (1.29)	1.88 (1.88)
5.77	ebp (φ =7.5°)	1.83 (1.82)	4.26 (4.22)
5.77	ebp (φ =19.5°)	1.83 (1.82)	6.51 (6.45)
	ep (φ =7.5°)	1.29 (1.29)	1.61 (1.61)
	ep (φ =19.5°)	1.29 (1.29)	1.87 (1.87)
5.00	ebp (φ =7.5°)	2.23 (2.22)	4.81 (4.80)
	ebp (φ =19.5°)	2.22 (2.22)	7.66 (7.66)
	ep (φ =7.5°)	1.49 (1.49)	1.59 (1.61)
	ep (φ =19.5°)	1.49 (1.49)	1.79 (1.86)

Note: ebp denotes the elastic–brittle–plastic model, and ep represents the elastic–plastic model

Table 2 Results of the plastic and softening radii and displacement

q (MPa)	Dilation angle	R/r_0	u/r_0 (%)
50.00	ebp (φ =0°)	2.556 (2.552)	2.624 (2.597)
	ebp(φ =19.5°)	2.556 (2.556)	6.403 (6.272)
	ep (φ =0°)	1.866 (1.858)	1.238 (1.217)
	ep (φ =19.5°)	1.8646 (1.858)	1.812 (1.891)
44.16	ebp (φ =0°)	2.192 (2.192)	2.253 (2.250)
	ebp (φ =19.5°)	2.192 (2.192)	4.844 (4.790)
	ep (φ =0°)	1.652 (1.652)	1.088 (1.086)
	ep (φ =19.5°)	1.652 (1.652)	1.605 (1.595)
35.00	ebp (φ =0°)	2.192 (2.192)	2.117 (2.095)
	ebp (φ =19.5°)	2.192 (2.192)	4.206 (4.003)
	ep (φ =0°)	1.652 (1.652)	1.050 (1.041)
	ep (φ =19.5°)	1.652 (1.652)	1.464 (1.450)
22.50	ebp (φ =0°)	2.192 (2.192)	2.051 (2.037)
	ebp (φ =19.5°)	2.192 (2.192)	3.992 (3.970)
	ep (φ =0°)	1.652 (1.652)	1.043 (1.033)
	ep (φ =19.5°)	1.652 (1.652)	1.444 (1.431)
15.83	ebp (φ =0°)	2.192 (2.192)	2.032 (2.019)
	ebp (φ =19.5°)	2.192 (2.192)	3.969 (3.953)
	ep (φ =0°)	1.652 (1.652)	1.047 (1.033)
	ep (φ =19.5°)	1.652 (1.652)	1.442 (1.431)
15.00	ebp (φ =0°)	2.390 (2.391)	2.102 (2.106)
	ebp (φ =19.5°)	2.390 (2.391)	4.389 (4.321)
	ep (φ =0°)	1.759 (1.759)	1.091 (1.037)
	ep (φ =19.5°)	1.759 (1.759)	1.433 (1.433)
14.00	ebp (φ =0°)	2.657 (2.657)	2.142 (2.142)
	ebp (φ =19.5°)	2.642 (2.642)	4.54 (4.487)
	ep (φ =0°)	1.927 (1.927)	1.026 (1.034)
	ep (φ =19.5°)	1.922 (1.922)	1.470 (1.432)

Note: ebp denotes the elastic–brittle–plastic model, and ep represents the elastic–plastic model

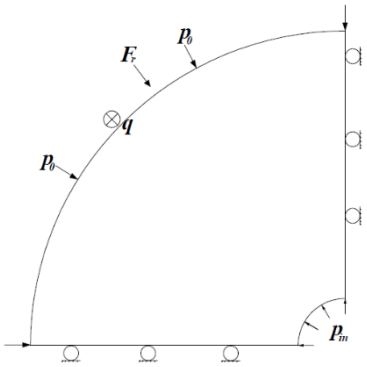

(a) Constraints and external force conditions

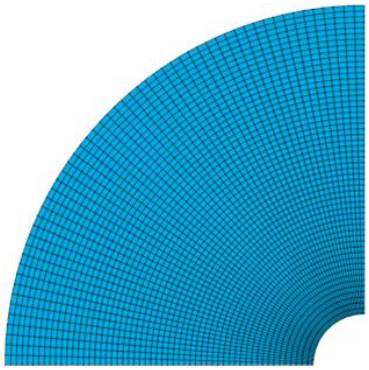

(b) Model mesh for quarter of opening

Fig. 5 The numerical simulation model for analysis

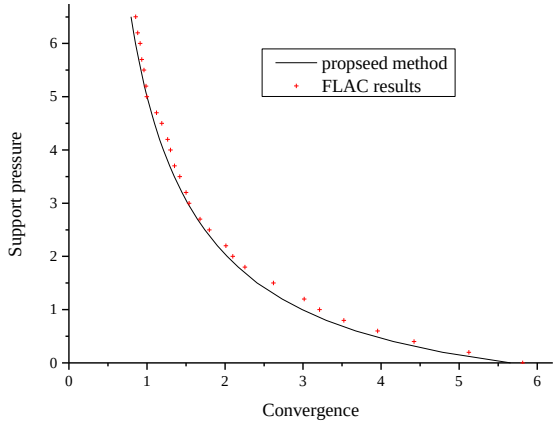

(a) M–C

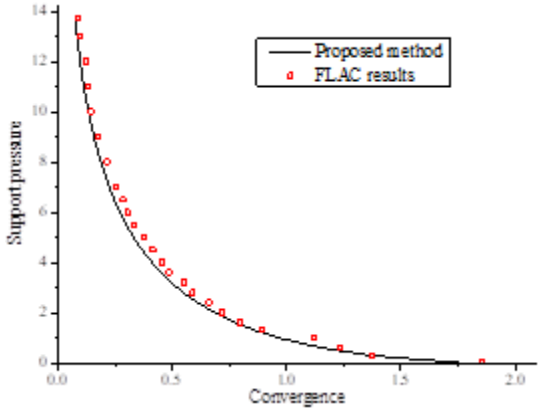

(b) Generalized H–B

Fig. 6 Results of the proposed solution and FLAC for the elastic–brittle–plastic model

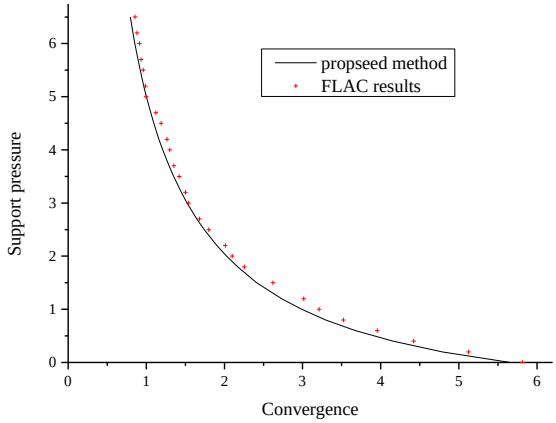

(a) M–C

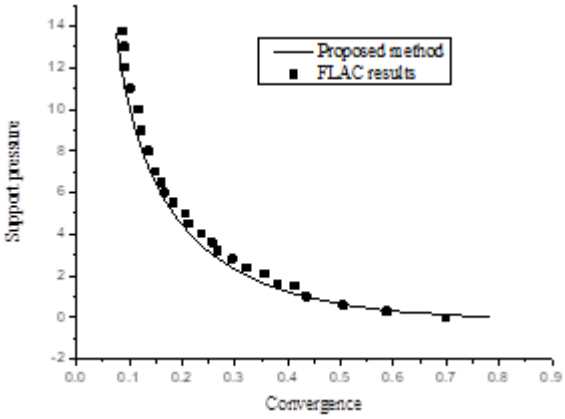

(b) Generalized H–B

Fig. 7 Results of the proposed solution and FLAC for the strain-softening model

is adopted from Wang *et al.* (2012) as follows: r_0 = 3.0 m, σ_0 = 30 MPa, p_{in} = 0 MPa, E= 27.0 GPa, υ = 0.22, c = 1.5 MPa, c_r = 0.7 MPa, ϕ = 50.9°, ϕ_r = 39° and φ = 7.5° (or 19.5°). The results of the proposed approach and those of Wang's solution (enclosed in parentheses) are presented in Table 1 for n = 1000 with different out-of-plane stresses (e.g., 60, 54.22, 30, 13.2, 5.77 and 5.0 MPa).

Table 1 shows that the results of the proposed approach agree well with those in Wang *et al.* (2012). Furthermore, the maximum difference $((u-u_{exact})/u_{exact}\times\%)$ is less than 0.208%. The proposed approach can also be transformed to Wang's solutions with F_r=0 and γ^{p*}=0 under M-C criterion.

For the generalized H–B failure criterion, the following parameters for surrounding rock are adopted: r_0=5 m , σ_0 = 30 MPa, p_{in} = 5 MPa, E=5.5 GPa, υ = 0.25, ψ=0°, σ_{cr} =30 MPa, m_b=1.7, a=0.55, s=0.0039, m_{br}=0.85, s_r=0.0019, a_r=0.6, r_ω=0.01, ξ=1, and h_a-h_0=50 m. A comparison of the results from this study and Wang's solution (enclosed in parentheses) is presented in Table 2 for n = 1000.

As shown in Table 2, the results of

$(u-u_{exact})/u_{exact}\times 100\%$ are less than 5.2% (Table 2). Therefore, the differences are sufficiently small when the high non-linearity of the generalized H–B failure criterion is considered.

After the validation of the proposed analytical model by comparing with the solutions from Wang *et al.* (2012), the proposed approach is compared with numerical results in this section. To validate the analytical model, the results of the analytical model are compared with those obtained from numerical simulation computations. Based on the axisymmetric boundary conditions in this study, quarter of opening and surrounding rock is built in model instead of the whole opening. The applied constraints and external force conditions are shown in Fig. 5(a). The adopted method of numerical simulation for strain-softening surrounding rock is presented in Guan *et al.* (2007) except the deviatoric plastic strain in Eq. (2b) is selected as the softening parameter in this study. The results for elastic–brittle–plastic model can be obtained by setting $\gamma^{p*}=0$.

This model was made up of 3000 zones as a plane strain model with the plane of analysis oriented normal to the axis of the hole. The results for the elastic–brittle–plastic and strain-softening models are shown in Figs. 6 and 7, respectively.

Tables 1 and 2 and Figs. 6 and 7 show that the results of the proposed approach are consistent with those of both Wang *et al.* (2012) and FLAC for both the elastic–brittle–plastic model and the strain-softening model.

5. Conclusions

This study presents a simple numerical method to calculate the displacement and stress of surrounding rock and determines the relationships of the out-of-plane stress and the major, intermediate and minor principle stresses for strain-softening surrounding rock. The study further considers the out-of-plane stress and the seepage force based on Biot's effective stress principle for the M–C and generalized H–B failure criteria. The elasto–perfectly plastic and the elasto–brittle–plastic models are special cases of the proposed approach. Compared with the previous results, the following improvements have been achieved.

(1) Incorporating the effects of the out-of-plane stress and seepage force, the new approach extends the application of cavity contraction theory in tunnel excavation based on Biot's effective stress principle. The rock effective coefficient is introduced as a correction coefficient that is independent of the effective stress.

(2) In the process of solving the stresses and displacements in the strain-softening surrounding rock, the strain-softening model is simplified as a multi-step brittle–plastic model, and the plastic region is divided into a number of concentric rings. In each ring, the strength parameters are assumed to be the same, and the continuity relations of stress and displacement are fulfilled.

(3) The proposed approach can describe the change of the stress distributions in the tunnel opening and provide a reference for design. When the directions of the principal tectonic stresses do not coincide with the axis of the underwater tunnel, we can apply the proposed approach in this situation to avoid the substantial error of ignoring the out-of-plane stress.

Additional work is planned to determine the possible range of the dilation angle and its influence on the evolution of the out-of-plane stress. This theory requires more verification in the context of practical engineering.

Acknowledgments

This research was supported by the Jiangxi Provincial Department of Communications Key Technology Foundation (No. 2020Z0001 and 2016C0007).

References

Aalianvari, A. (2017), "Combination of engineering geological data and numerical modeling results to classify the tunnel route based on the groundwater seepage", *Geomech. Eng.*, **13**(4), 671-683. https://doi.org/10.12989/gae.2017.13.4.671.

Aksoy, C.O., Aksoy, G.G., Guney, A., Ozacar, V. and Yaman, H.E. (2020), "Influence of time-dependency on elastic rock properties under constant load and its effect on tunnel stability", *Geomech. Eng.*, **20**(1), 1-7. https://doi.org/10.12989/gae.2020.20.1.001.

Alonso, E., Alejano, L.R., Varas, F., Fdez-Manín, G. and Carranza-Torres, C. (2003), "Ground response curves for rock masses exhibiting strain-softening behaviour", *Int. J. Numer. Anal. Meth. Geomech.*, **27**(13), 1153-1185. https://doi.org/10.1002/nag.315.

Atkinson, J.H. and Potts, D.M. (1977), "Stability of a shallow circular tunnel in cohesionless soil", *Geotechnique*, **27**(2), 203-215. https://doi.org/10.1680/geot.1977.27.2.203.

Biot, M.A. and Wills, D.G. (1957), "The elastic coefficients of the theory of consolidation", *J. Appl. Mech.*, **24**, 594-601.

Bobet, A. (2001), "Analytical solutions for shallow tunnels in saturated ground", *J. Eng. Mech.*, **127**(12), 1258-1266. https://doi.org/10.1061/(ASCE)0733-9399(2001)127:12(1258).

Brown, E.T., Bray, J.W., Ladanyi, B. and Hoek, E. (1983), "Ground response curves for rock tunnels", *J. Geotech. Eng.*, **109**(1), 15-39. https://doi.org/10.1061/(ASCE)0733-9410(1983)109:1(15).

Bui, T.A., Wong, H., Deleruyelle, F., Dufour, N., Leo, C. and Sun, D.A. (2014), "Analytical modeling of a deep tunnel inside a poro-viscoplastic rock mass accounting for different stages of its life cycle", *Comput. Geotech.*, **58**(5), 88-100. https://doi.org/10.1016/j.compgeo.2013.11.004.

Carranza-Torres, C. (2004), "Elasto-plastic solution of tunnel problems using the generalized form of the Hoek-Brown failure criterion", *Int. J. Rock Mech. Min. Sci.*, **41**(3), 480-481. https://doi.org/10.1016/j.ijrmms.2004.03.111.

Chen, G.H. and Zou, J.F. (2020), "Analysis of tunnel face stability with non-linear failure criterion under the pore water pressure", *Eur. J. Environ. Civ. Eng.*, 1-13. https://doi.org/10.1080/19648189.2020.1777905.

Chen, G.H., Zou, J.F. and Pan, Q.J. (2020), "Earthquake-induced slope displacements in heterogeneous soils with tensile strength cut-off", *Comput. Geotech.*, **124**, 103637. https://doi.org/10.1016/j.compgeo.2020.103637.

Cosenza, P., Ghoreychi, M., De Marsily, G., Vasseur, G. and Violette, S. (2002), "Theoretical prediction of poroelastic

properties of argillaceous", *Water Resour. Res.*, **38**(10), 25-1. https://doi.org/10.1029/2001WR001201.

Detournay, E. and Cheng, A.H.D. (1993), *Fundamentals of Poroelasticity*, in *Analysis and Design Methods*, Pergamon Press.

Farhadian, H., Hassani, A.N. and Katibeh, H. (2017), "Groundwater inflow assessment to Karaj Water Conveyance tunnel, northern Iran", *KSCE J. Civ. Eng.*, **21**(6), 2429-2438. https://doi.org/10.1007/s12205-016-0995-2.

Golpasand, M.R., Ngoc, A.D., Daniel, D. and Mohammad-Reza, N. (2018), "Effect of the lateral earth pressure coefficient on settlements during mechanized tunneling", *Geomech. Eng.*, **16**(6), 643-654. https://doi.org/10.12989/gae.2018.16.6.643.

Guan, Z., Jiang, Y., Tanabasi, Y. and Huang, H. (2007), "Reinforcement mechanics of passive bolts in conventional tunnelling", *Int. J. Rock Mech. Min. Sci.*, **44**(4), 625-636. https://doi.org/10.1016/j.ijrmms.2006.10.003.

Harr, M.E. (1962), *Groundwater and Seepage*, McGraw-Hill, New York, U.S.A.

Hoek, E., Carranza-Torres, C. and Corkum, B. (2002), "Hoek–Brown failure criterion-2002 edition", *Procedings of the North American Rock Mechanics Society Meeting*, Toronto, Canada, July.

Jeffery, G.B. (1921), "Plane stress and plane strain in bipolar co-ordinates", *Phil. Trans. Royal Soc. London Ser. A*, **221**(582-593), 265-293. https://doi.org/10.1098/rsta.1921.0009.

Lee, Y.K. and Pietruszczak, S. (2008), "A new numerical procedure for elasto-plastic analysis of a circular opening excavated in a strain-softening rock mass", *Tunn. Undergr. Sp. Technol.*, **23**(5), 588-599. https://doi.org/10.1016/j.tust.2007.11.002.

Lei, S. (1999), "An analytical solution for steady flow into a tunnel", *Ground Water*, **37**(1), 23-26. https://doi.org/10.1111/j.1745-6584.1999.tb00 953.

Li, W. and Zhang, C. (2020), "Face stability analysis for a shield tunnel in anisotropic sands", *Int. J. Geomech.*, **20**(5), 04020043. https://doi.org/10.1061/(ASCE)GM.1943-5622.0001666.

Mindlin, R.D. (1940), "Stress distribution around a tunnel", *T. Amer. Soc. Civ. Eng.*, **195**(1), 1117-1140.

Ogawa, T. and Lo, K.Y. (1987), "Effects of dilatancy and yield criteria on displacements around tunnels", *Can. Geotech. J.*, **24**(1), 100-113. https://doi.org/10.1139/t87-009.

Park, K.H., Tontavanich, B. and Lee, J.G. (2008), "A simple procedure for ground response curve of circular tunnel in elastic-strain softening rock masses", *Tunn. Undergr. Sp. Technol.*, **23**(2), 151-159. https://doi.org/10.1016/j.tust.2007.03.002.

Pinto, F. and Whittle, A.J. (2013), "Ground movements due to shallow tunnels in soft ground. I: Analytical solutions", *J. Geotech. Geoenviron. Eng.*, **140**(4), 04013040. https://doi.org/10.1061/(ASCE)GT.1943-5606. 0000948.

Qian, Z.H., Zou, J.F., Tian, J. and Pan, Q.J. (2020), "Estimations of active and passive earth thrusts of non-homogeneous frictional soils using a discretisation technique", *Comput. Geotech.*, **119**(3), 103366. https://doi.org/10.1016/j.compgeo.2019.103366.

Rezaei Amir, H., Mojtaba, S., Mohammad, R. and Baghban, G. (2019), "EPB tunneling in cohesionless soils: A study on Tabriz Metro settlements", *Geomech. Eng.*, **19**(2), 153-165. https://doi.org/10.12989/gae.2019.19.2.153.

Schleiss, A. (1986), "Design of previous pressure tunnels", *Int. Water Power Dam Construct.*, **38**(5), 21-26.

Wang, S.L., Wu, Z., Guo M.W. and Ge, X.R. (2012), "Theoretical solutions of a circular tunnel with the influence of out-of-plane stress in elastic-brittle-plastic rock", *Tunn. Undergr. Sp. Technol.*, **30**(4), 155-168. https://doi.org/10.1016/j.tust.2012.02.016.

Xiao, Y. and Liu, H. (2017), "Elastoplastic constitutive model for rockfill materials considering particle breakage", *Int. J. Geomech.*, **17**(1), 04016041. https://doi.org/10.1061/(ASCE)GM.1943-5622.0000681.

Xiao, Y., Chen, H., Stuedlein, A.W., Evans, T.M., Chu, J., Cheng, L., Jiang, N., Lin, H., Liu, H. and Aboel-Naga, H.M. (2020), "Restraint of particle breakage by biotreatment method", *J. Geotech. Geoenviron. Eng.*, **146**. https://doi.org/10.1061/(ASCE)GT.1943-5606.0002384.

Xiao, Y., Meng, M., Daouadjie, A., Chen, Q., Wu, Z. and Jiang, X. (2020), "Effect of particle size on crushing and deformation behaviors of rockfill materials", *Geosci. Front.*, **11**(2), 375-388. https://doi.org/10.1016/j.gsf.2018.10.010.

Xiao, Y., Sun, Y., Yin, F., Liu, H. and Xiang, J. (2017), "Constitutive modeling for transparent granular soils", *Int. J. Geomech.*, **17**(7), 04016150. https://doi.org/10.1061/(ASCE)GM.1943-5622.0000857.

Zhang, C., Han, K. and Zhang, D. (2015), "Face stability analysis of shallow circular tunnels in cohesive–frictional soils", *Tunn. Undergr. Sp. Technol.*, **50**, 345-357. https://doi.org/10.1016/j.tust.2015.08.007.

Zhang, C., Li, W., Zhu, W. and Tan, Z. (2020), "Face stability analysis of a shallow horseshoe-shaped shield tunnel in clay with a linearly increasing shear strength with depth", *Tunn. Undergr. Sp. Technol.*, **97**, 103291. https://doi.org/10.1016/j.tust.2020.103291.

Zou, J.F. and Zuo, S.Q. (2017), "Similarity solution for the synchronous grouting of shield tunnel under the vertical nonaxisymmetric displacement boundary condition", *Adv. Appl. Math. Mech.*, **9**(1), 205-232. https://doi.org/10.4208/aamm.2016.m1479.

Zou, J.F., Sheng, Y.M., Xia, M.Y. and Wang, F. (2020), "A novel numerical-iterative-approach for strain-softening surrounding rock incorporating rockbolts effectiveness and hydraulic-mechanical coupling based on Three-Dimensional Hoek-Brown strength criterion", *Tunn. Undergr. Sp. Technol.*, **101**(7), 103358. https://doi.org/10.1016/j.tust.2020.103358.

Zou, J.F., Wei A. and Li, L. (2020), "Analytical solution for steady seepage and groundwater inflow into an underwater tunnel", *Geomech. Eng.*, **20**(3), 267-273. https://doi.org/10.12989/gae.2020.20.3.267.

GC